

Chapter 4

CoP As An Acid-Stable Active Electrocatalyst For The Hydrogen-Evolution Reaction: Electrochemical Synthesis, Interfacial Characterization And Performance Evaluation

Saadi, F. H.; Carim, A. I.; Verlage, E.; Hemminger, J. C.; Lewis, N. S.; Soriaga, M. P. *The Journal of Physical Chemistry C* **2014**, *118*, 29294. DOI: 10.1021/jp5054452

4.1 Introduction

The previous two chapters have focused on acid-stable, earth-abundant HER catalysts that consist of Group VI transition metals and chalcogenides. Another family of promising hydrogen evolution catalysts that was discovered during my time at Caltech is the transition metal phosphide group. Recently, crystalline nanoparticles of Ni₂P, MoP, and CoP have been reported as acid-compatible HER catalysts that exhibit low overpotentials in acidic electrolytes.¹⁶⁻²¹ Additionally, Ni-P and Co-P alloys have been studied as alkaline-stable HER catalysts, although the exact compositions and activities were irreproducible among different samples.²²⁻²⁶ In this chapter we describe a facile electrochemical method for the synthesis of a cobalt phosphide film that displays high HER activity and significant *operando* acid-stability.

4.2 Cobalt phosphide electrodeposition and characterization

4.2.1 Characterization of films prior to electrocatalysis

Scanning-electron micrographs (SEM) of the as-deposited thin film (Figures 4.1A, 4.1B, and 4.1C) showed the surfaces to be relatively smooth but with micron-sized spherical clusters randomly and loosely distributed throughout. Energy-dispersive X-ray spectroscopy (EDS) indicated that the surface was composed primarily of cobalt and a minor amount of phosphorous in a Co:P ratio of 20:1 (Figure 4.2). EDS also yielded the same 20:1 ratio for the clusters.

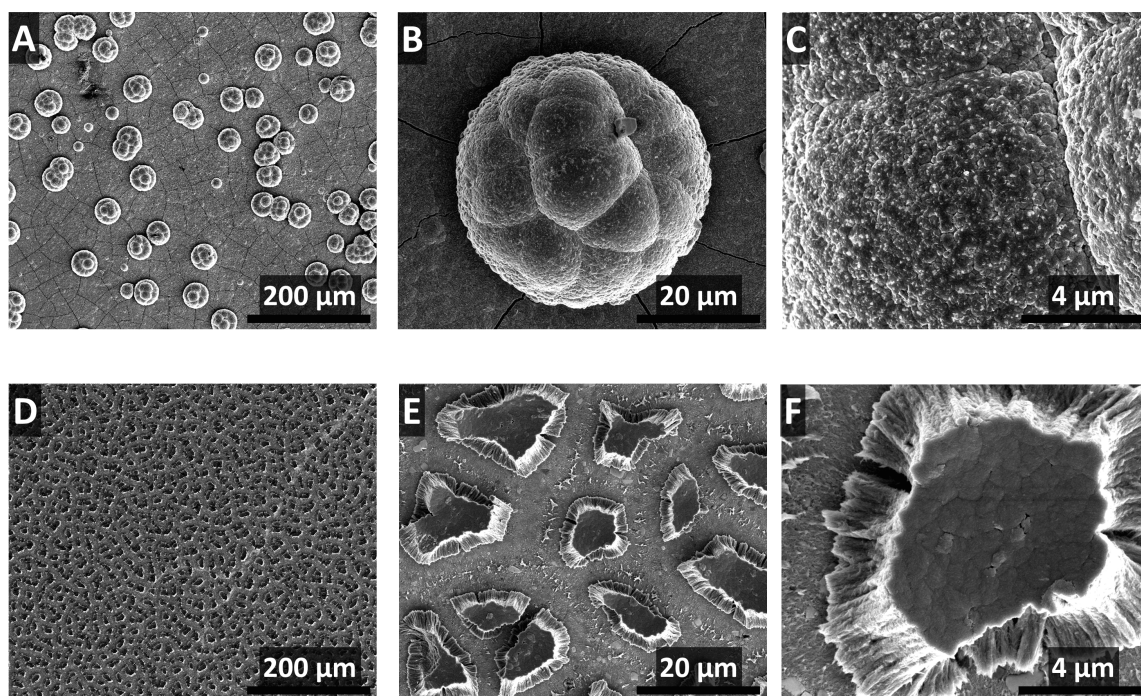


Figure 4.1: Scanning-electron micrographs of the films before (A, B, and C) and after (D, E, and F) voltammetry. A: An As-deposited thin film showed the presence of quasi-spherical clusters on the surface. B and C: The film underneath the particles appeared

uniformly roughened. D: Post-electrolysis film showed close-packed plateau-topped islands on the surface. E and F: The tops of the mesa-like islands were flat and relatively smooth.

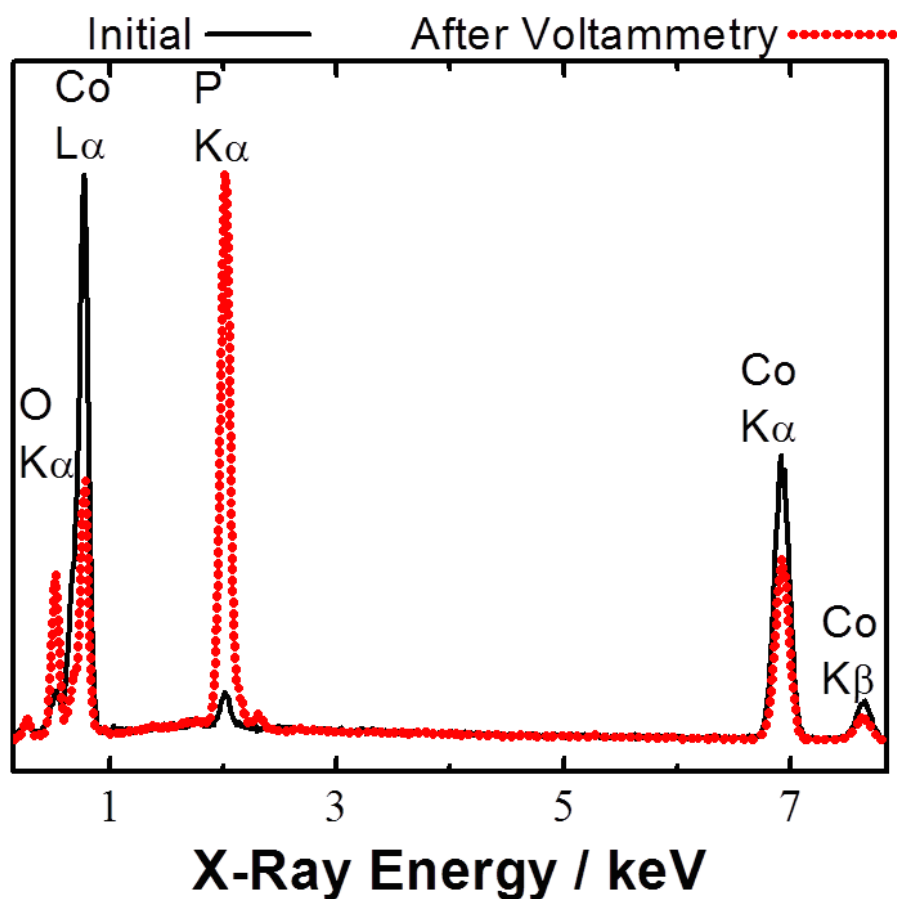


Figure 4.2: Energy-dispersive X-ray spectroscopy of the films before and after voltammetry. The Co:P atomic ratio decreased from 20:1 to 1:1 after the voltammetric experiments.

Figures 4.3A and 4.3B show high-resolution X-ray photoelectron spectra of the samples in the Co and P regions, respectively. The peaks at 778 eV and 793 eV in Figure

4.3A correspond to the $2p_{3/2}$ and $2p_{1/2}$ peaks of zerovalent Co. All of the other peaks are associated with oxidized cobalt, Co_3O_4 ($\text{CoO}\cdot\text{Co}_2\text{O}_3$).²⁸⁻³¹ The large peak in Figure 4.3B at 133 eV is assigned to orthophosphate, probably as the cobalt salt $\text{Co}_3(\text{PO}_4)_2$.^{32,33} The observed broadening is consistent with an unresolved overlap of the $2p_{3/2}$ and $2p_{1/2}$ states.³⁴ Based on Equation (4.1), the Co:P atomic ratio was determined to be 8:1. The latter is considerably smaller than the EDS-determined ratio (20:1) because X-rays emanate deeper from the sample bulk compared to photoemitted electrons. This difference in the Co:P ratio implies surface segregation of phosphorus in the as-prepared sample.

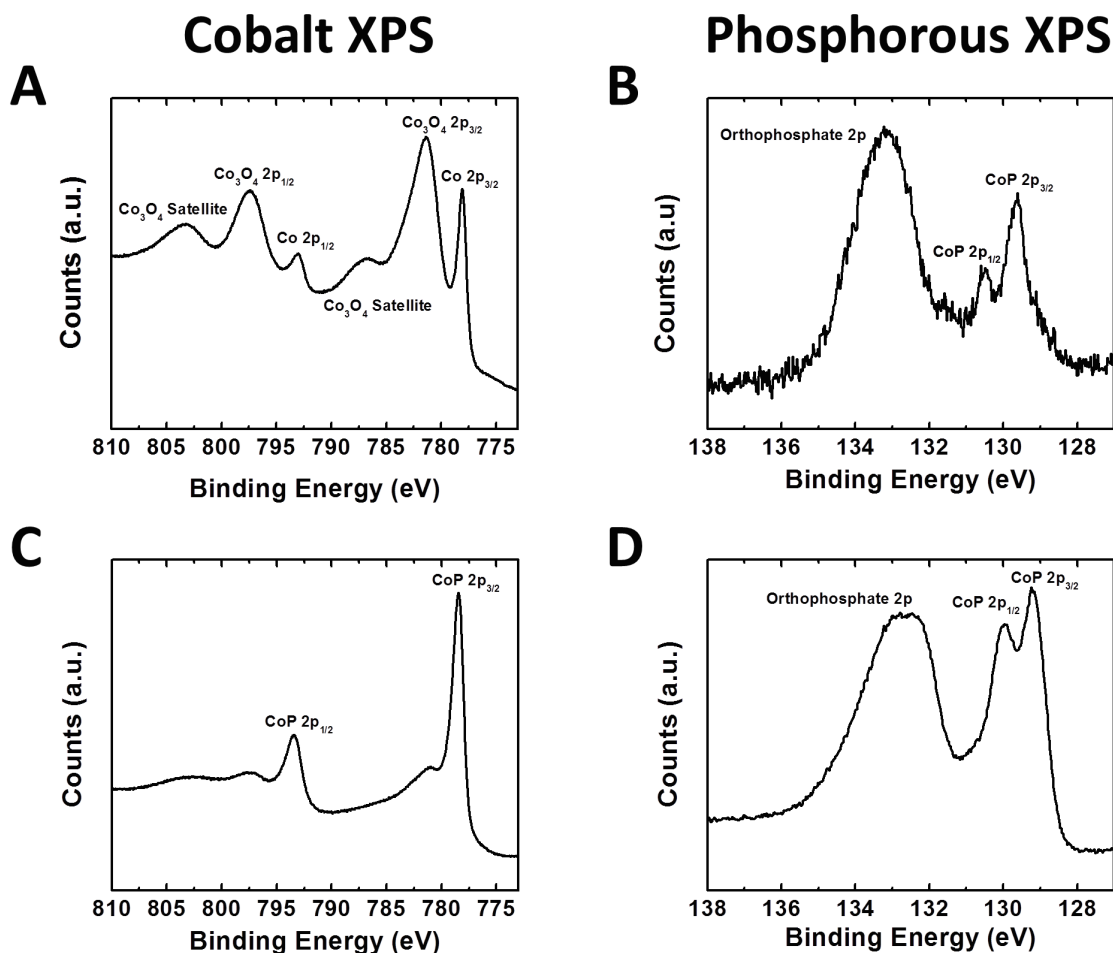


Figure 4.3: High-resolution X-ray photoelectron spectra of (A) Co 2p region of the as-deposited thin film; (B) P 2p region of the as-deposited thin film; (C) Co 2p region after voltammetry; (D) P 2p region after voltammetry.

The Raman spectrum of the as-deposited cobalt phosphide film (Figure 4.4) exhibited a broad, asymmetric band centered at 590 cm^{-1} which is characteristic of amorphous cobalt oxide³⁵. The shoulders at 487 , 522 , and 690 cm^{-1} are consistently assigned to Co_3O_4 stretching modes (E_g , F_{2g} , and A_{1g}).³⁶ Additional peaks at 925 , 981 and 1067 cm^{-1} were also observed and are consistent with P-O stretching modes (ν_1 symmetric, ν_1 symmetric, and ν_3 anti-symmetric respectively).^{37,38}

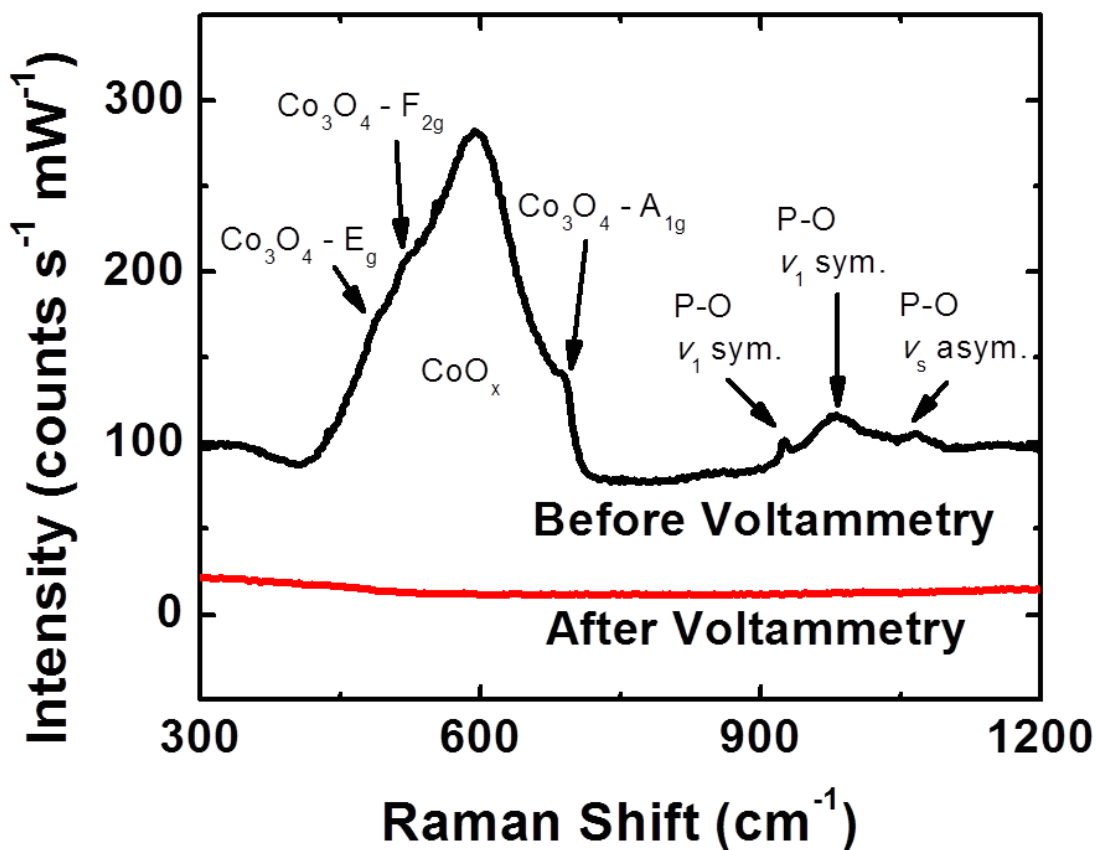


Figure 4.4: Raman spectra before and after voltammetry. The peaks at *ca.* 600 cm^{-1} correspond to Co-O vibrational modes, whereas those at *ca.* 1100 cm^{-1} are attributable to P-O modes.

4.2.2 Electrochemistry

Figure 4.5 displays the cyclic current vs. potential data for the cobalt phosphide thin film in aqueous 0.500 M H_2SO_4 . In the first scan (Figure 4.5A), initially from the open-circuit potential (-0.075 V) to 0.025 V vs RHE, a large anodic current was observed that was not replicated in subsequent runs. After that first cycle, in all experiments, the overpotential (η) needed to drive 10 mA cm^{-2} of cathodic current was 85 mV (RHE). This overpotential was significantly lower than those observed for the Co-on-Cu and pure-Cu control experiments (Figure 4.5B). Figure 4.5C shows a representative steady-state Tafel plot for the cobalt-phosphide film, which yielded a slope of 50 mV dec^{-1} and an exchange current density of 0.20 mA cm^{-2} . Figure 4.5D compares the Tafel plot of the subject compound with those of other HER catalysts. Only platinum outperformed the electrodeposited cobalt-phosphide film under the stated test conditions.

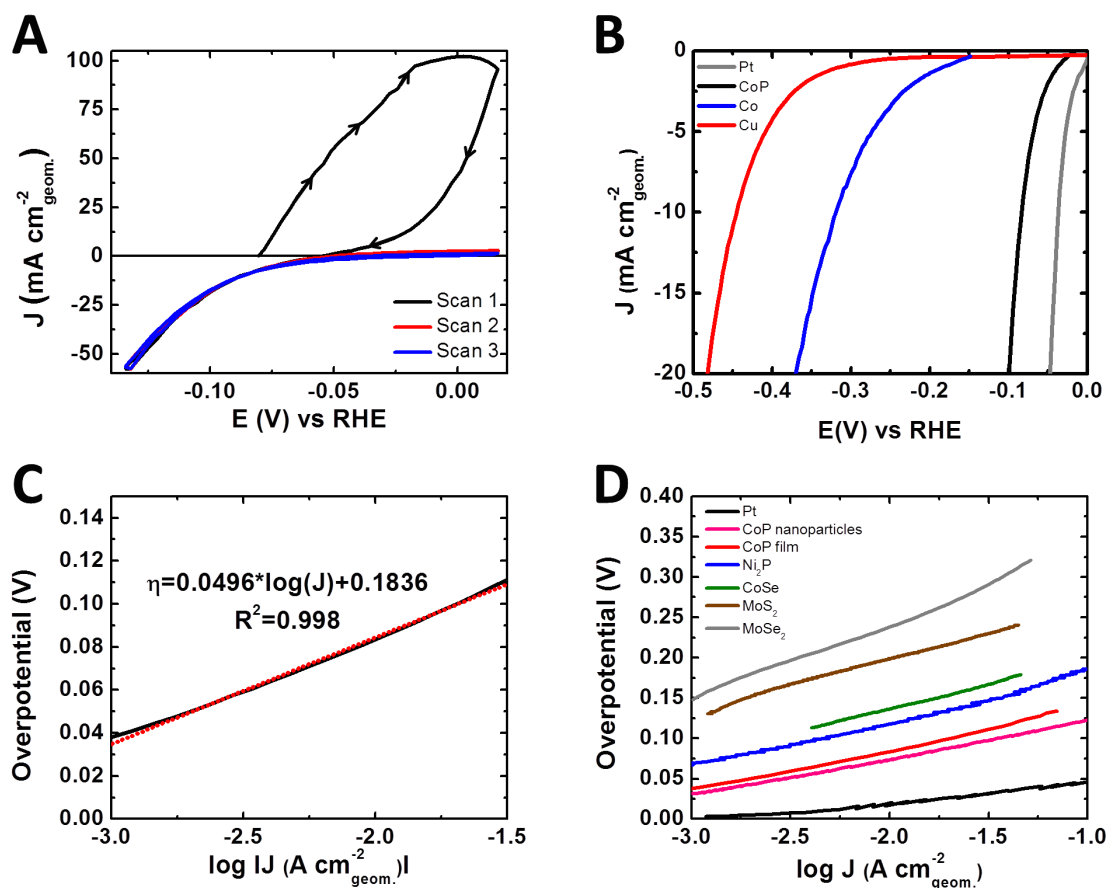


Figure 4.5: (A) Cyclic voltammetric data for cobalt phosphide thin films on glassy carbon in aqueous 0.50 M H₂SO₄. (B) Current density vs potential data for Pt (gray), the third scan of CoP (black), Co (blue) and Cu (red). (C) Tafel plot of CoP from the current density vs potential data in (B). (D) Tafel plots that compare the activity of the film in 0.50 M H₂SO₄ with that of Pt,²¹ CoP nanoparticles,²¹ Ni₂P nanoparticles,²⁰ CoSe thin films,⁴¹ MoSe₂ thin films,⁴² and MoS₂ thin films.⁹

Two methods were implemented to assess the *operando* stability of the catalytically active film in highly acidic environments. In one, the sample was cycled,

uninterrupted, between 0.0 V and -0.14 V vs RHE in 0.5 M H₂SO₄ for 24 h and the ensuing cyclic voltammogram (CV) was compared with that for first cycle (Figure 4.6A). The CV data indicated an increase in η from 85 mV to 100 mV after the day-long test. The other stability-assessment method was based on chronopotentiometry, in which a constant current density of 10 mA cm⁻² was delivered over 24 h while the electrode potential, i.e. the value of η , was monitored (Figure 4.6B). The average increase in η from the two methods was 17.5 ± 4.5 mV.

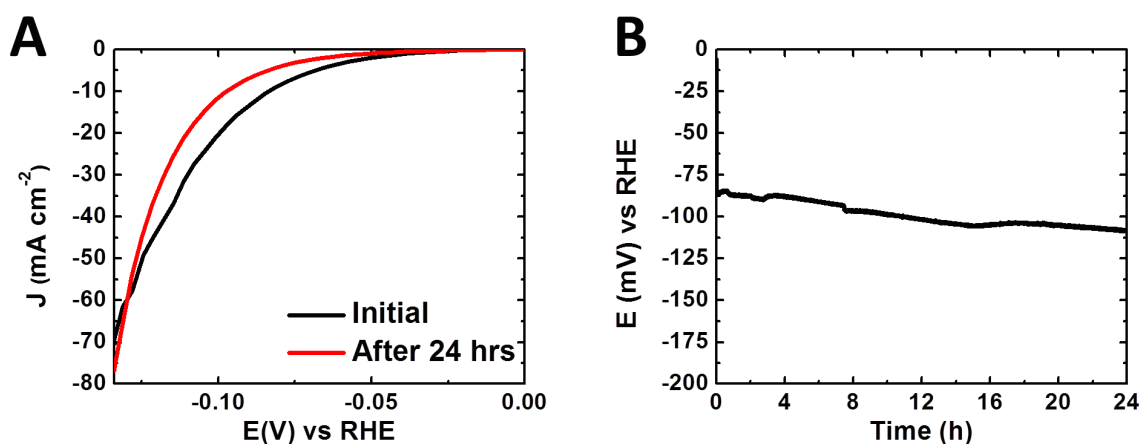


Figure 4.6: (A) Current density vs potential data in 0.50 M H₂SO₄, for the first cycle and after uninterrupted scans over 24 h. (B) Chronopotentiometry in 0.50 M H₂SO₄ at a constant current density of 10 mA cm⁻².

4.2.3 Post-electrochemistry film characterization

Figures 4.1D, 4.1E, and 4.1F show SEM images of the film obtained after the HER catalysis experiments. The most notable difference between these images and the pre-electrochemistry images of Figures 4.1A, 4.1B, and 4.1C is that the film surface was

no longer marred with loosely distributed quasi-spheres but was instead covered with close-packed plateau-topped particles that resembled micron-sized mesas. The tops of the mesa-like particles were relatively flat and smooth. Post-electrochemistry EDS measurements (Figure 4.2) indicated that Co:P ratio in the film decreased twenty-fold to 1:1.

Figures 4.3C and 4.3D, respectively, show high-resolution XPS spectra of the sample in the Co and P regions. Comparison of Figure 4.3C with Figure 4.3A clearly indicates that all peaks attributable to cobalt oxides have diminished; the two major peaks represent Co 2p_{3/2} and Co 2p_{1/2} states in the stoichiometric CoP.^{21,32,39} Close inspection of Figures 4.3B and 4.3D reveals that the relative intensities of the post-electrochemistry phosphide peaks at 129 and 131 eV increased, whereas that of the phosphate peak at 133 eV decreased significantly. Based on Equation (4.1), the atomic ratio of cobalt and phosphorous after the hydrogen-evolution experiments decreased from 8:1 to 1:1, in agreement with the EDS results.

The Raman spectrum (Figure 4.4) after electrochemistry showed the absence of peaks at 600 cm⁻¹, thus providing clear evidence that the catalytically active film did not contain cobalt oxide.

4.3 Discussion

When a clean copper disk electrode is immersed in an aqueous solution of 0.15 M H₃BO₃, 0.10 M NaCl, 0.30 M NaPO₂H₂, and 0.2 M CoCl₂ and applied with a potential of -1.2 V, the following deposition reactions are expected to occur:⁴⁰





A spontaneous Co-P compound formation reaction then occurs to give the net reaction:



While a few stoichiometric compositions of cobalt phosphide are known (e.g., Co_3P and Co_2P),^{25,32} the 1:1 ratio explicitly shown in Equation (4.2) is based upon the post-electrocatalysis XPS, and EDS results. The as-deposited film, whether examined by EDS, XPS or Raman spectroscopy, showed a preponderance of higher-valent Co and P species such as Co_2O_3 , CoO , and orthophosphate salts. This behavior may be a consequence of the air-oxidation of the sample when removed from the deposition solution, rinsed with Nanopure water, and transferred to the XPS instrument.

The large anodic current observed in the first voltammetric cycle is consistent with expectations for the quantitative anodic dissolution of metallic cobalt to the divalent cation, Co^{2+} , which is desorbed into solution. Under HER conditions, dissolution of CoO and Co_2O_3 evidently also takes place as indicated by the complete loss of cobalt oxides, as well as by the significant decrease in the Co:P atomic ratio observed in the post-catalysis XPS and EDS data. The magnitude of the orthophosphate XPS peak in the as-prepared sample was substantially diminished after the HER cycles. This decrease was consistent with expectations for the cathodic reduction of interfacial orthophosphate species; when the film was removed from solution, in the absence of applied potential, the reduced products readily reverted to the orthophosphates. Thus, *ex-situ* surface spectroscopy showed non-zero, but substantially diminished, orthophosphate coverage; this is as expected for samples that were briefly exposed to air during sample transfer. The net result is an example of an *operando* purification, with the deposit changing

chemically from a composite of active and inert substances to solely the catalytically functional material.

For the electrodeposited cobalt phosphide film, spectral results from XPS showed that the binding energy of cobalt was significantly lower than either the Co^{2+} or Co^{3+} species. This is to be expected since a previous study on metal monophosphides has revealed the covalent nature of the cobalt-phosphorous bond.³⁹ The covalently bonded CoP is better represented as $\text{Co}^{\delta+}\text{P}^{\delta-}$, where $\delta+$ and $\delta-$ denote partial, non-integer, charges; consequently, the Co peaks would be closer to those of the zerovalent metal. If the interaction between cobalt and phosphorus were purely ionic, the designation would have been $[\text{Co}^{3+}][\text{P}^{3-}]$, and the Co peak would be that for the Co^{3+} species.

The overpotential (η) necessary to deliver a proton-reduction current density of 10 mA cm^{-2} , a catalytic-activity metric that is an order of magnitude higher than in natural photosynthesis, was 85 mV for electrodeposited CoP. In addition, the CoP electrodeposits displayed stability in acidic environments, in that after 24 h of uninterrupted HER-voltammetric cycles, η increased by only $17.5 \pm 4.5 \text{ mV}$. The results for the electrodeposited CoP micron-sized particles are comparable to those obtained using CoP nanoparticles.²¹ In terms of η , the comparative catalytic performance of the CoP film is as follows (Figure 4.5): $\eta_{\text{Pt}} < \eta_{\text{CoP Film}} = \eta_{\text{CoP NP}}, \eta_{\text{Ni}_2\text{P}} < \eta_{\text{CoSe}_2} < \eta_{\text{MoS}_2} < \eta_{\text{MoSe}_2}$.

4.4 Conclusion

Cobalt phosphide was prepared, as a film on a copper substrate, by cathodic deposition from a boric acid solution of Co^{2+} and H_2PO_2^- . Surface structural and

compositional analysis of the film prior to the electrocatalysis measurements indicated that the film consisted of micron-sized spherical clusters located randomly and loosely on a slightly rough surface. The composition of both the clusters and surface consisted of cobalt in the metallic, phosphide, and amorphous-oxide forms ($\text{CoO}\cdot\text{Co}_2\text{O}_3$), and of phosphorus as phosphide and orthophosphate. The higher-valent species that originated from air-oxidation were remediated upon HER electrocatalysis in sulfuric acid. The *operando* film purification yielded a functional electrocatalyst with a Co:P stoichiometric ratio of 1:1. The post-HER surface was densely packed with micron-sized mesa-like particles whose tops were flat and smooth. The CoP electrodeposit showed an overvoltage of 85 mV at a current density of 10 mA cm^{-2} , and exhibited *operando* stability in acidic solution, characterized by an increase in η of 18 mV after 24 h of uninterrupted operation. In terms of η , the comparative catalytic performance of CoP is: $\eta_{\text{Pt}} < \eta_{\text{CoP Film}} \leq \eta_{\text{CoP NP}}$, $\eta_{\text{Ni}_2\text{P}} < \eta_{\text{CoSe}_2} < \eta_{\text{MoS}_2} < \eta_{\text{MoSe}_2}$.

4.5 Experimental

All chemical reagents were analytical grade and used without further purification. Ultra-clean water with resistivity higher than $18.2 \text{ M}\Omega \text{ cm}$ was generated from a Barnstead Nanopure system (Thermo Scientific, Asheville, NC). Unless otherwise specified, all experiments were performed under ambient laboratory conditions.

Rotating-disk electrode substrates. Copper disks (Alfa Aesar, Ward Hill, MA) that were used as deposition substrates were 5 mm diameter, 4 mm thickness, and 99.999 % purity. The disks were metallographically burnished on a LaboPol-5 polisher (Struers

Inc., Cleveland, OH), initially with 15- μ SiC (Buehler, Lake Bluff, IL) and subsequently with progressively decreased grit size (9, 6, 3 to 1 μ) diamond paste. The disks were then cleaned with a 0.06- μ colloidal suspension of silica and sonicated for 5 min in Nanopure water.

Electrochemistry. Electrochemical experiments were performed in a 100-mL four-port glass cell that was equipped with a 99%-pure graphite rod (Alfa Aesar) that served as a counter electrode, and a saturated calomel electrode (SCE) (CH Instruments, Austin, TX) as reference. The SCE was calibrated (266 mV) against a reversible hydrogen electrode (RHE) in 0.5 M H₂SO₄. Potential control was accomplished with a BioLogic SP-200 potentiostat (Biologic, Grenoble, France). The uncompensated cell resistance was determined from a single-point high-frequency impedance measurement and was compensated (85 %) by the built-in positive-feedback software.

The cobalt phosphide film was electrodeposited onto a Cu disk from a 250-mL solution that consisted of 0.928 g (0.15 M) of boric acid, H₃BO₃, (Alfa Aesar), 0.584 g (0.10 M) sodium chloride, NaCl, (Macron Fine Chemicals, Center Valley, PA), 3.48 g (0.30 M) sodium hypophosphite, NaPO₂H₂, Alfa Aesar) and 4.759 g (0.2 M) cobalt chloride, CoCl₂, (Alfa Aesar). The pH of the solution, prior to and after the electrodeposition experiments, was 5.0. The rotating disk electrode (RDE) was rotated at a frequency of 6.67 Hz (400 rpm) with the potential maintained at -1.2 V vs SCE for 15 min. For control experiments, a cobalt-only film was prepared based on the same procedure but in the absence of NaPO₂H₂.

Hydrogen-evolution catalysis measurements were performed in a 0.50 M H₂SO₄ solution that was prepared from 18 M H₂SO₄ (Sigma Aldrich, St. Louis, MO) by use of

ultrapure water. In the HER experiments, the solution and the RDE cell were saturated with 99.999 % H₂(g) (Air Liquide, Plumsteadville, PA) and the RDE was rotated at 26.67 Hz (1600 rpm). Voltammetric data were obtained by cycling the potential between 0.0 V and -0.14 V vs RHE at a scan rate of 1 mV s⁻¹. The *operando* stability of the films was evaluated by continuous cyclic voltammetry over a 24 h period. Chronopotentiometry at constant current density of 10 mA cm⁻² was also performed during which the potential of the cobalt phosphide film was monitored over a 24 h period.

Interfacial Characterization

Scanning-electron micrographs were obtained using a Nova NanoSEM 450 microscope (FEI, Hillsboro, OR) with an accelerating voltage of 15 kV and a working distance of 5.0 mm. Low-magnification micrographs (> 10 nm per pixel) were acquired with an Everhart-Thornley detector whereas higher-magnification micrographs were obtained with a through-the-lens detector. Energy-dispersive X-ray spectra (EDS) were collected in the SEM at an accelerating voltage of 15 kV using a silicon drift detector (Oxford Instruments, Abingdon, United Kingdom). Inca software (Oxford Instruments, Abingdon, United Kingdom) was used to interpret the EDS spectra.

XPS data were obtained using an AXIS Ultra DLD instrument (Kratos Analytical, Manchester, UK) at a background pressure of 1×10^{-9} Torr. High-intensity excitation was provided by monochromatic Al K α X-rays, 1486.6 eV in energy and 0.2-eV resolution at full width at half maximum. Photoelectrons were collected at 0° from the surface normal at a retarding (pass) energy of 80 eV for the survey scans, whereas a pass energy of 20 eV was used for the high-resolution scans. The peak energies were calibrated against the binding energy E_B of the adventitious C 1s peak. For quantitative analysis, the XPS peaks

were fitted using CasaXPS software (CASA Ltd, Teignmouth, United Kingdom) to symmetric Voigt line shapes composed of Gaussian (70%) and Lorentzian (30%) functions that employed a Shirley background.²⁷ For both the Co and P peaks, the fitting was constrained to maintain a 2:1 ratio between the areas of the 2p_{3/2} and 2p_{1/2} peaks, with E_B separations of 0.85 eV and 15 eV for P and Co, respectively. The atomic or molar ratio between Co and P was obtained from Equation (4.1):

$$\frac{N_{\text{Co}}}{N_{\text{P}}} = \frac{A_{\text{Co}}/S_{\text{Co}}}{A_{\text{P}}/S_{\text{P}}} \quad (4.1)$$

where N is the number of atoms, A is the total area of the photoemission peaks, and S the sensitivity factor. Values for S (0.486 for P and 3.59 for Co) were provided by the instrument manufacturer.

Raman spectra of the films were obtained with a Renishaw inVia Raman microprobe (Renishaw, Wotton Under Edge, United Kingdom) equipped with a Leica DM 2500M microscope (Leica Microsystems, Buffalo Grove, IL), a Leica N Plan 50x objective (numerical aperture = 0.75), a 1800 lines mm⁻¹ grating and a CCD detector configured in a 180° backscatter geometry. A 532-nm diode-pumped solid-state laser (Renishaw RL532C50) was used as the excitation and a 20-μW radiant flux was incident onto the surface of the sample.

4.6 References

- (1) Lewis, N. S.; Nocera, D. G. Powering the Planet: Chemical Challenges in Solar Energy Utilization. *Proc. Natl. Acad. Sci. U. S. A.* **2006**, *103*, 15729-15735.
- (2) Lewis, N. S. Toward Cost-Effective Solar Energy Use. *Science* **2007**, *315*, 798-801.
- (3) Turner, J.; Sverdrup, G.; Mann, M. K.; Maness, P.-C.; Kroposki, B.; Ghirardi, M.; Evans, R. J.; Blake, D. Renewable Hydrogen Production. *Int. J. Energ. Res.* **2008**, *32*, 379-407.
- (4) Walter, M. G.; Warren, E. L.; McKone, J. R.; Boettcher, S. W.; Mi, Q.; Santori, E. A.; Lewis, N. S. Solar Water Splitting Cells. *Chem. Rev. (Washington, DC, U. S.)* **2010**, *110*, 6446-6473.
- (5) Gray, H. B. Powering the Planet with Solar Fuel. *Nature Chem.* **2009**, *1*, 7-7.
- (6) Merki, D.; Hu, X. Recent Developments of Molybdenum and Tungsten Sulfides as Hydrogen Evolution Catalysts. *Energy Environ. Sci.* **2011**, *4*, 3878-3888.
- (7) Laursen, A. B.; Kegnæs, S.; Dahl, S.; Chorkendorff, I. Molybdenum Sulfides—Efficient and Viable Materials for Electro - and Photoelectrocatalytic Hydrogen Evolution. *Energy Environ. Sci.* **2012**, *5*, 5577-5591.
- (8) Vrubel, H.; Hu, X. Growth and Activation of an Amorphous Molybdenum Sulfide Hydrogen Evolving Catalyst. *ACS Catal.* **2013**, 2002-2011.
- (9) Benck, J. D.; Chen, Z.; Kuritzky, L. Y.; Forman, A. J.; Jaramillo, T. F. Amorphous Molybdenum Sulfide Catalysts for Electrochemical Hydrogen Production: Insights into the Origin of Their Catalytic Activity. *ACS Catal.* **2012**, *2*, 1916-1923.

- (10) Kibsgaard, J.; Chen, Z.; Reinecke, B. N.; Jaramillo, T. F. Engineering the Surface Structure of MoS₂ to Preferentially Expose Active Edge Sites For electrocatalysis. *Nat. Mater.* **2012**, *11*, 963-969.
- (11) Bonde, J.; Moses, P. G.; Jaramillo, T. F.; Nørskov, J. K.; Chorkendorff, I. Hydrogen Evolution on Nano-Particulate Transition Metal Sulfides. *Faraday Discuss.* **2009**, *140*, 219-231.
- (12) Kong, D.; Wang, H.; Cha, J. J.; Pasta, M.; Koski, K. J.; Yao, J.; Cui, Y. Synthesis of MoS₂ and MoSe₂ Films with Vertically Aligned Layers. *Nano Lett.* **2013**, *13*, 1341-1347.
- (13) Velazquez, J. M.; Saadi, F. H.; Pieterick, A. P.; Spurgeon, J. M.; Soriaga, M. P.; Brunshwig, B. S.; Lewis, N. S. Synthesis and Hydrogen-Evolution Activity of Tungsten Selenide Thin Films Deposited on Tungsten Foils. *J. Electroanal. Chem.* **2014**, *716*, 45-48.
- (14) Kong, D.; Cha, J. J.; Wang, H.; Lee, H. R.; Cui, Y. First-Row Transition Metal Dichalcogenide Catalysts for Hydrogen Evolution Reaction. *Energy Environ. Sci.* **2013**, *6*, 3553-3558.
- (15) Chen, W. F.; Wang, C. H.; Sasaki, K.; Marinkovic, N.; Xu, W.; Muckerman, J. T.; Zhu, Y.; Adzic, R. R. Highly Active and Durable Nanostructured Molybdenum Carbide Electrocatalysts for Hydrogen Production. *Energy Environ. Sci.* **2013**, *6*, 943-951.
- (16) Liu, Q.; Tian, J.; Cui, W.; Jiang, P.; Cheng, N.; Asiri, A. M.; Sun, X. Carbon Nanotubes Decorated with CoP Nanocrystals: A Highly Active Non-Noble-Metal Nanohybrid Electrocatalyst for Hydrogen Evolution. *Angew. Chem.* **2014**

- (17) Tian, J.; Liu, Q.; Asiri, A. M.; Sun, X. Self-Supported Nanoporous Cobalt Phosphide Nanowire Arrays: An Efficient 3D Hydrogen-Evolving Cathode over the Wide Range of pH 0–14. *J. Am. Chem. Soc.* **2014**, *136*, 7587-7590.
- (18) Wang, X.; Xiao, P.; Thia, L.; Alam Sk, M.; Lim, R. J.; Ge, X.; Wang, J.-Y.; Lim, K. H. Molybdenum Phosphide as an Efficient Electrocatalyst for Hydrogen Evolution Reaction. *Energy Environ. Sci.* **2014**.
- (19) Feng, L.; Vrubel, H.; Bensimon, M.; Hu, X. Easily-Prepared Dinickel Phosphide (Ni₂P) Nanoparticles as an Efficient and Robust Electrocatalyst for Hydrogen Evolution. *Phys. Chem. Chem. Phys.* **2014**, *16*, 5917-5921.
- (20) Popczun, E. J.; McKone, J. R.; Read, C. G.; Biacchi, A. J.; Wiltrout, A. M.; Lewis, N. S.; Schaak, R. E. Nanostructured Nickel Phosphide as an Electrocatalyst for the Hydrogen Evolution Reaction. *J. Am. Chem. Soc.* **2013**, *135*, 9267-9270.
- (21) Popczun, E. J.; Read, C. G.; Roske, C. W.; Lewis, N. S.; Schaak, R. E. Highly Active Electrocatalysis of the Hydrogen Evolution Reaction by Cobalt Phosphide Nanoparticles. *Angewandte Chemie International Edition* **2014**, *53*, 5427-5430.
- (22) Burchardt, T. The Hydrogen Evolution Reaction on NiP_x Alloys. *Int. J. Hydrogen Energy* **2000**, *25*, 627-634.
- (23) Burchardt, T.; Hansen, V.; Våland, T. Microstructure and Catalytic Activity Towards the Hydrogen Evolution Reaction of Electrodeposited NiP_x Alloys. *Electrochim. Acta* **2001**, *46*, 2761-2766.
- (24) Paseka, I. Evolution of Hydrogen and Its Sorption on Remarkable Active Amorphous Smooth Ni-P(X) Electrodes. *Electrochim. Acta* **1995**, *40*, 1633-1640.

- (25) Paseka, I.; Velicka, J. Hydrogen Evolution and Hydrogen Sorption on Amorphous Smooth Me-P(X) (Me=Ni, Co and Fe-Ni) Electrodes. *Electrochim. Acta* **1997**, *42*, 237-242.
- (26) Morikawa, T.; Nakade, T.; Yokoi, M.; Fukumoto, Y.; Iwakura, C. Electrodeposition of Ni-P Alloys from Ni-Citrate Bath. *Electrochim. Acta* **1997**, *42*, 115-118.
- (27) Shirley, D. A. High-Resolution X-ray Photoemission Spectrum of the Valence Bands of Gold. *Phys. Rev. B* **1972**, *5*, 4709-4714.
- (28) Biesinger, M. C.; Payne, B. P.; Grosvenor, A. P.; Lau, L. W. M.; Gerson, A. R.; Smart, R. S. C. Resolving Surface Chemical States in XPS Analysis of First Row Transition Metals, Oxides and Hydroxides: Cr, Mn, Fe, Co and Ni. *Appl. Surf. Sci.* **2011**, *257*, 2717-2730.
- (29) McIntyre, N. S.; Cook, M. G. X-Ray Photoelectron Studies on Some Oxides and Hydroxides of Cobalt, Nickel, and Copper. *Anal. Chem.* **1975**, *47*, 2208-2213.
- (30) McIntyre, N. S.; Johnston, D. D.; Coatsworth, L. L.; Davidson, R. D.; Brown, J. R. X-ray Photoelectron Spectroscopic Studies of Thin Film Oxides of Cobalt and Molybdenum. *Surf. Interface Anal.* **1990**, *15*, 265-272.
- (31) Tan, B. J.; Klabunde, K. J.; Sherwood, P. M. A. XPS Studies of Solvated Metal Atom Dispersed (SMAD) Catalysts. Evidence for Layered Cobalt-Manganese Particles on Alumina and Silica. *J. Am. Chem. Soc.* **1991**, *113*, 855-861.
- (32) Nemoshalenko, V. V.; Didyk, V. V.; Senekevich, A. I. *Russ. J. Org. Chem.* **1983**, *28*, 2182.
- (33) Cobo, S.; Heidkamp, J.; Jacques, P.-A.; Fize, J.; Fourmond, V.; Guetaz, L.; Joussetme, B.; Ivanova, V.; Dau, H.; Palacin, S.; Fontecave, M.; Artero, V. A Janus

Cobalt-Based Catalytic Material for Electro-Splitting of Water. *Nat. Mater.* **2012**, *11*, 802-807.

(34) Okamoto, Y.; Nitta, Y.; Imanaka, T.; Teranishi, S. Surface Characterisation of Nickel Boride and Nickel Phosphide Catalysts by X-ray Photoelectron Spectroscopy. *Journal of the Chemical Society, Faraday Transactions 1: Physical Chemistry in Condensed Phases* **1979**, *75*, 2027-2039.

(35) Tyczkowski, J.; Kapica, R.; Łojewska, J. Thin Cobalt Oxide Films for Catalysis Deposited by Plasma-Enhanced Metal–Organic Chemical Vapor Deposition. *Thin Solid Films* **2007**, *515*, 6590-6595.

(36) Hadjiev, V. G.; Iliev, M. N.; Vergilov, I. V. The Raman Spectra of Co_3O_4 . *J. Phys. C* **1988**, *21*, L199.

(37) Frost, R. L. An Infrared and Raman Spectroscopic Study of Natural Zinc Phosphates. *Spectrochimica Acta Part A: Molecular and Biomolecular Spectroscopy* **2004**, *60*, 1439-1445.

(38) Mitchell, P. C. H.; Parker, S. F.; Simkiss, J.; Simmons, J.; Taylor, M. G. Hydrated Sites in Biogenic Amorphous Calcium Phosphates: An Infrared, Raman, and Inelastic Neutron Scattering Study. *J. Inorg. Biochem.* **1996**, *62*, 183-197.

(39) Grosvenor, A. P.; Wik, S. D.; Cavell, R. G.; Mar, A. Examination of the Bonding in Binary Transition-Metal Monophosphides MP (M = Cr, Mn, Fe, Co) by X-ray Photoelectron Spectroscopy. *Inorg. Chem.* **2005**, *44*, 8988-8998.

(40) Plambeck, J. A.; Bard, A. J.; Henning, L. Encyclopedia of Electrochemistry of the Elements. Vol. 3 Vol. 3, 1973.

(41) Carim, A. I.; Saadi, F. H.; Soriaga, M. P.; Lewis, N. S. Electrocatalysis of the Hydrogen-Evolution Reaction by Electrodeposited Amorphous Cobalt Selenide Films. *J. Mater. Chem. A* **2014**, *2*, 13835-13839.

(42) Saadi, F. H.; Carim, A. I.; Velazquez, J. M.; Baricuatro, J. H.; McCrory, C. C. L.; Soriaga, M. P.; Lewis, N. S. Operando Synthesis of Macroporous Molybdenum Diselenide Films for Electrocatalysis of the Hydrogen-Evolution Reaction. *ACS Catal.* **2014**, 2866-2873.